

# Hygroscopic Growth and Deliquescence of NaCl Nanoparticles Coated with Surfactant AOT<sup>†</sup>

Ahmad Alshawa,<sup>‡,§</sup> Otto Dopfer,<sup>||</sup> Christopher W. Harmon,<sup>‡,§</sup> Sergey A. Nizkorodov,<sup>\*,§</sup> and Joelle S. Underwood<sup>§,⊥</sup>

Department of Chemistry, University of California, Irvine, California 92697-2025, and Institut fuer Optik und Atomare Physik, Technische Universitaet Berlin, Hardenbergstrasse 36, D-10623 Berlin, Germany

Received: November 09, 2008; Revised Manuscript Received: February 13, 2009

Aerosolized nanoparticles of NaCl coated with variable amounts of surfactant AOT were generated by electrospraying AOT/NaCl aqueous solutions, followed by neutralizing and drying the resulting particles. A tandem differential mobility analyzer was used to select a narrow size distribution of particles with mobility equivalent diameters below 20 nm and monitor their hygroscopic growth as a function of relative humidity. Effects of the particle size and relative amount of surfactant on the hygroscopic growth of NaCl were studied. For pure NaCl nanoparticles, the deliquescence relative humidity (DRH) increased as the particle size was decreased, in full agreement with previous measurements. Below the DRH the NaCl nanoparticles had an equivalent of one–four monolayers of water adsorbed on the surface. The addition of a sub-monolayer AOT coating reduced the DRH and suppressed the hygroscopic growth of the NaCl core. At AOT coverage levels exceeding one monolayer, a clear deliquescence transition was no longer discernible. The Zdanovskii–Stokes–Robinson (ZSR) model failed to predict the observed growth factors of mixed AOT/NaCl nanoparticles reflecting a large contribution of the interfacial interactions between NaCl and AOT to the total free energy of the particles. There were indications that AOT/NaCl nanoparticles prepared by the electrospray aerosol source were enhanced in the relative mass fraction of AOT in comparison with the solution from which they were electrosprayed.

## Introduction

Atmospheric nanoparticles, also known as ultrafine particles,<sup>1</sup> are typically defined as particles with aerodynamic diameters below 100 nm. The physical basis for this size threshold is the unique ability of such particles to translocate through biological tissues.<sup>2,3</sup> Atmospheric nanoparticles are directly emitted by a number of sources, such as diesel engines,<sup>4</sup> and can also be produced by condensation of molecular precursors during particle nucleation events.<sup>5</sup> Once formed, they undergo deposition onto larger particles and other available surfaces on time scales ranging from several seconds to several hours.<sup>6</sup> Despite their relatively short atmospheric lifetimes, nanoparticles dominate the number concentration and make a significant contribution to the available surface area of particulate matter.<sup>1,7</sup> The high surface-to-volume ratio of nanoparticles strongly favors atmospheric chemistry that is specific to the particle surfaces.<sup>8,9</sup>

Atmospheric particles can significantly expand in size by taking up water as the relative humidity (RH) increases. This hygroscopic growth increases the particle's single scattering albedo and plays an important role in cloud droplet formation.<sup>10,11</sup> Hygroscopicity of individual particles is normally quantified in terms of the growth factor (GF), the ratio of the measured particle mobility diameter ( $d_m$ ) at a certain RH to that of the dry particle.<sup>12</sup>

$$GF_{\text{mobility}} = \frac{d_m^{\text{wet}}}{d_m^{\text{dry}}} \quad (1)$$

The extent and rate of the hygroscopic growth is a sensitive function of both the particle's initial diameter and the chemical composition. For highly soluble inorganic particles, such as NaCl, and certain highly soluble organic particles, such as malonic acid, GF may experience a discontinuity at a well-defined deliquescence relative humidity (DRH) corresponding to a phase transition from a solid to a dissolved state.<sup>11,13–16</sup> The reverse phase transition occurs at the efflorescence relative humidity (ERH), which can be considerably lower than DRH because of kinetic constraints. For example, NaCl particles experience almost no growth below its DRH of 75%.<sup>17</sup> At the DRH point, NaCl particles undergo a transition from its crystalline form into an aqueous droplet, which is accompanied by a prompt increase in the particle mobility diameter. The ERH for NaCl occurs at ~45%.<sup>18</sup>

This study focuses on hygroscopic properties of nanoparticles with sizes below ~20 nm, which are interesting for a number of fundamentally important reasons.<sup>19</sup> In this size range, there is a nontrivial contribution of the surface energy to the free energy of the particle:

$$G_{\text{particle}} = \mu_{\text{bulk}} n_{\text{bulk}} + \mu_{\text{surface}} n_{\text{surface}} \approx \mu_{\text{bulk}} n_{\text{bulk}} + \sigma_{\text{surface}} A_{\text{particle}} \quad (2)$$

$G$ ,  $\mu$ ,  $n$ ,  $\sigma$ , and  $A$  stand for free energy, chemical potential, molar amount, surface tension, and particle surface area, respectively.

<sup>†</sup> Part of the "Robert Benny Gerber Festschrift".

\* Corresponding author, nizkorod@uci.edu.

<sup>‡</sup> Graduate students who made equal contributions to this project.

<sup>§</sup> University of California, Irvine.

<sup>||</sup> Technische Universitaet Berlin.

<sup>⊥</sup> Current address: Department of Chemistry, Loyola University, New Orleans, LA 70118.

In other words, the surface energy term in the free energy expression, which can be safely neglected for particles larger than 100 nm, starts to be comparable in magnitude to the bulk free energy contribution.<sup>20–24</sup> As a result of the large surface-to-volume ratios of nanoparticles, their GF, ERH, and DRH values can be size-dependent.

Only a few experimental and theoretical studies of hygroscopic growth of nanoparticles are currently available. Hämeri et al.<sup>25–27</sup> were the first to measure GF for 8–60 nm NaCl and (NH<sub>4</sub>)<sub>2</sub>SO<sub>4</sub> particles. They found that GF increases with increasing particle size and that the DRH for NaCl particles in this size range is higher than DRH for larger particles.<sup>17</sup> They also observed “nonprompt” (gradual) deliquescence, a concept first described in a theoretical study of deliquescence of small particles by Mirabel.<sup>20</sup> A modeling study by Russell and Ming<sup>22</sup> expanded on Mirabel’s work and showed that the observed sign and magnitude of the DRH shift in small NaCl particles is consistent with deliquescence of NaCl nanocrystals precoated with a thin layer of water (as opposed to completely dry particles below DRH assumed in ref 20).

More recent measurements by Biskos et al.<sup>28–30</sup> challenged the nonpromptness of the deliquescence and showed that it can be attributed to the experimental artifacts in the operation of the tandem differential mobility analyzer used for these measurements. Contrary to the previous theoretical predictions,<sup>20,22</sup> they could only observe the nanosize effect on DRH for NaCl particles but not for (NH<sub>4</sub>)<sub>2</sub>SO<sub>4</sub> particles. Gao et al.<sup>18</sup> modeled the efflorescence of NaCl nanoparticles by combining the Köhler equation with homogeneous nucleation theory and correctly predicted the increase in ERH values for smaller particle sizes observed in ref 29.

As the particle size approaches molecular dimensions, the macroscopic description of phase transitions should become less meaningful. However, even for the smallest 6 nm particles of NaCl and (NH<sub>4</sub>)<sub>2</sub>SO<sub>4</sub> studied in refs 25, 26, 29, and 30, the GF values observed above DRH could still be accurately predicted using thermodynamic parameters appropriate for bulk samples after accounting for the particle shape effects.<sup>28,30</sup> The observed particle size dependence of the DRH could also be modeled using standard thermodynamics approaches without having to resort to a molecular level description of the phase transitions.<sup>22</sup> It was possible to use a macroscopic description for the theoretical prediction of phase transitions in even smaller particles (down to 2 nm in size) by allowing for phenomenological size dependence of the surface tension.<sup>23,31</sup>

Atmospheric particles generally represent complicated mixtures of organic and inorganic species with very different levels of water solubility. To better understand the consequences of having poorly miscible species in the same particle, hygroscopic properties of particles with inorganic core–organic shell morphologies were investigated by several groups.<sup>12,32–34</sup> The organic material did not appear to inhibit the growth of the soluble inorganic core, even for cases when the organic material was the dominant constituent of particles.<sup>12,32</sup> Measured GF values for the mixed particles were approximately consistent with the assumption that the organic and inorganic species adsorb water independently, in accordance with the Zdanovskii–Stokes–Robinson (ZSR) model.<sup>33,34</sup> Similar conclusions were reached in studies of water activities above the bulk mixtures of the same compounds.<sup>35,36</sup> The main objective of this work is to test the effect of sparingly soluble organic coatings on hygroscopic properties of NaCl nanoparticles. To ensure that the organic layer is confined to the surface, we chose AOT, sodium bis(2-ethylhexyl) sulfosuccinate (Figure 1), a well-

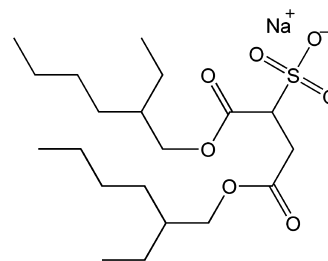


**Figure 1.** Sodium bis(2-ethylhexyl) sulfosuccinate (AOT): C<sub>20</sub>H<sub>37</sub>NaO<sub>7</sub>S, CAS 577-11-7, MW 444.56 g/mol.

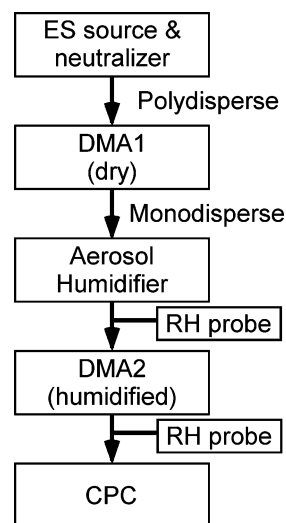


**Figure 2.** Experimental approach for generating, size selecting, conditioning, and monitoring hygroscopic growth of nanoparticles. Key: RH, relative humidity; DMA, differential mobility analyzer; CPC, condensation particle counter; ES, electrospray.

known surfactant with a strong propensity for forming inverted micelles in condensed phase.<sup>37–39</sup>

## Experimental Methods

Figure 2 shows an experimental schematic for generating nanoparticles and monitoring their hygroscopic growth. Nanoparticles containing NaCl and AOT were generated with a home-built electrospray aerosol source. Variable amounts of NaCl (Sigma-Aldrich, 99.999%) and AOT (Fluka, ≥99.0%) were dissolved in deionized HPLC grade water (OmniSolv, <8 μΩ·cm) to achieve a combined concentration of ~1 g/L. A small amount (<5%) of methanol (Sigma-Aldrich, HPLC grade, >99.9%) was added to the solution in order to enhance the electrospray cone stability. The solution was pushed through a 5 cm long, 100 μm i.d. quartz capillary with a syringe pump (780100 KD Scientific) at a typical flow rate of ~1 μL/min. High voltage (2–3 kV) was applied directly to the stainless steel needle of the syringe (Hamilton GT, 500 μL). The capillary entered a small (~5 cm<sup>3</sup>) chamber equipped with transparent windows for easy viewing of the electrospray jet with a microscope objective and CCD camera. The end of the capillary was positioned 3–5 mm away from the electrically grounded 6 mm o.d. entrance tube of a bipolar neutralizer (<sup>85</sup>Kr, 10 mCi, TSI model 3054). A ~1 SLM (standard liter per minute) flow of dry air was sent into the chamber to help with carrying the aerosol into the neutralizer.

The electrospray source produced particle concentrations in excess of 10<sup>6</sup> particles per cm<sup>3</sup> in a relatively narrow distribution of particle sizes characterized by geometric standard deviations

(GSD) of  $\sim 1.2$ . The particles were free of the residual solvents (see discussion below). Mean particle diameter could be varied from 5 to 30 nm by adjusting the solution concentration and solution flow rate. For each size, the electrospray voltage had to be adjusted for optimal stability. For this size range, more than 90% of the particles are expected to be uncharged after the neutralization step, which establishes a near-Boltzmann distribution of charges on the particles.<sup>40</sup> The rest of the particles should be singly charged, with a negligible contribution ( $<1\%$ ) from multiply charged particles.<sup>41</sup> For comparison purposes, pure NaCl particles were also generated by vaporization and condensation of solid NaCl as described by Fuks.<sup>42</sup> This method produced higher concentrations of particles ( $\sim 10^7 \text{ cm}^{-3}$ ) than the electrospray source but it could not be used for making AOT/NaCl mixed particles.

A 0.30–0.40 SLM flow coming from the electrospray source was directed into the first differential mobility analyzer (DMA1, TSI 3085). The applied dc voltage in DMA1 was fixed to allow a narrower distribution (GSD  $\sim 1.05$ ) of particle mobility diameters to pass through (at the expense of losing  $\sim 99\%$  of the uncharged particles). The DMA1 sheath flow (3.0–4.0 SLM) was operated with a closed loop configuration in which the excess air was filtered twice, dried with a Nafion dryer (PermaPure, MD-110), and recirculated. The resulting RH of the sheath flow was approximately 1–3%.

Size selected particles were brought to a desired RH by using a Nafion humidifier (Perma Pure, MD-110-48E-F) which consisted of a 2 mm wide, 120 cm long Nafion tube carrying the aerosol flow placed inside a 6 mm ID plastic tube carrying humidified air in the opposite direction. A rapid and stable adjustment of a desired RH inside the Nafion humidifier was achieved by mixing highly humidified air (RH  $>95\%$ ) and dry air in different proportions. RH was monitored by Vaisala HMP237 probes, which were periodically calibrated against RH above standard saturated salt solutions. The best achievable accuracy and precision of the probes were  $\pm 1.0\%$  RH and  $\pm 0.1\%$  RH, respectively, in the 0–90% RH range.

Humidified particles were sized in the second nano-DMA (DMA2, TSI 3085) operated in a scanning mode, and counted by a condensation particle counter (CPC, TSI 3025A). The estimated residence time of particles in the humidified flow (Nafion tube + RH probe + DMA2) was  $\sim 5$  s. The sheath air of DMA2 (3.0–4.0 SLM; 10:1 sheath:aerosol flow ratio) had a closed loop configuration with an independent control of RH, which was adjusted by mixing humid (RH  $>95\%$ ) and dry air in different proportions. The excess air was filtered twice and heat exchanged to match the sheath air temperature, which was typically 22 °C. RH was monitored by a separate calibrated Vaisala HMP237 probe. As a matter of experimental convenience, the DMA2 sheath flow was maintained at a level that was slightly higher than that of the aerosol flow, typically by 0–3% RH. When the difference between the DMA2 sheath flow and the aerosol flow RH was larger than zero, the final particle growth took place inside the DMA2 sheath air. All growth factors measured in this work are presented as a function of the sheath flow RH encountered by the particles in DMA2.

In most measurements, the RHs of the aerosol and DMA2 flows were slowly increased in parallel. The electrospray source was operated continuously, and the final particle size distributions were measured several times after the RH values stabilized at a desired level. Readings from all RH probes were continuously monitored by a computer. It took approximately 2 to 3 days to record each growth curve over a 5–90% RH range. After a 12 h period it was usually necessary to stop the

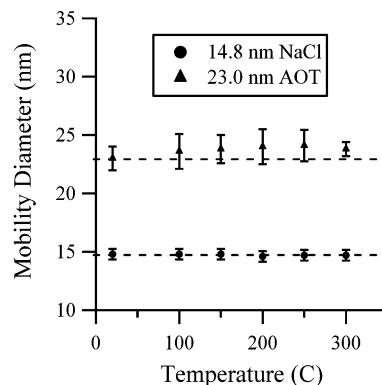


**Figure 3.** Mean particle sizes for pure NaCl and AOT aerosol as a function of temperature at the entrance of a diffusion drier. Error bars are  $3\sigma$  from repeated measurements.

electrospray source and clean the neutralizer from solid AOT/NaCl deposits forming at its entrance tube. In order to achieve reproducibility in the measured GF and DRH values, it was critical to keep both DMAs and all aerosol tubing free of contamination by volatile organics, especially for measurements on pure NaCl particles.

## Results

**Characterization of Particles.** To confirm that particles produced by the electrospray source were free of the residual solvent, the particle size distribution was measured before and after they passed through a diffusion drier with a resistively heated inlet. For this measurement, the initial particle size was not preselected with DMA1. Figure 3 shows the mean geometric size of pure NaCl and AOT particles as a function of the inlet temperature. As the temperature is increased from 25 to 300 °C, no distinctive change in the mean size is observed for the NaCl and AOT particles within the experimental uncertainties in the measured mobility equivalent diameters ( $3\sigma$  error bars are shown in Figure 3). The uncertainties are somewhat larger for AOT compared to NaCl because the former has a somewhat broader particle size distribution.

An SEM/TEM (scanning/transmission electron microscopy) grid was immersed in the aerosol flow directly after the neutralizer for several minutes. Collected particles composed of pure AOT were imaged with SEM and TEM. The images of isolated particles revealed that they were spherical, with the observed diameters being consistent with the mobility equivalent diameters measured by the DMA apparatus. A number of AOT particles appeared to conglomerate with each other on the grids, but the individual particles retained their initial shape within the conglomerates. The particles were stable under the vacuum conditions of the electron microscope chamber. These observations provided additional confirmation that the particles were essentially solvent-free.

We have attempted to quantify the relative AOT and NaCl mass fractions in the particles generated by the electrospray aerosol source by collecting the AOT/NaCl particles and measuring the sulfur-to-chlorine ratio with X-ray photoelectron spectroscopy (XPS) methods. The results were not conclusive due to the small mass of collected material. In this paper, we assume that the relative NaCl and AOT mass fractions in the particles are approximately the same as in the original solution. However, we discuss possible deviations from this assumption at the end of this paper.

**Hygroscopic Growth of Pure NaCl Nanoparticles.** NaCl was selected as the inorganic core material for these experiments

**TABLE 1: Shape Corrections for the Measured Growth Factors of NaCl Particles**

$d_m^{\text{dry}}$ (nm)	$Kn$	$\chi(Kn)$	$d_{ve}$ (nm)
9.0	14.7	1.25 <sup>a</sup>	8.1
10.8	12.2	1.25	9.7
10.9	12.1	1.25	9.8
14.0	9.43	1.23 <sup>b</sup>	12.5
14.1	9.36	1.23	12.7
17.0	7.76	1.23	15.2

<sup>a</sup> Calculated from Dahneke et al.<sup>68–70</sup> <sup>b</sup> Calculated in this work by methods of DeCarlo et al.<sup>52</sup>

because of the wide availability of experimental and theoretical data on wetting of pure NaCl nanoparticles,<sup>18,20,22–30</sup> larger NaCl particles,<sup>13,16,17,43–45</sup> and NaCl surfaces (only a few selected references are cited here).<sup>46–51</sup> A number of reference experiments on pure NaCl nanoparticles were conducted in order to validate the operation of the tandem nano-DMA apparatus.

Dry NaCl particles have a cubic shape,<sup>45</sup> whereas the deliquesced NaCl particles are spherical. In order to accurately quantify the degree of the particle hygroscopic growth, the observed GF values must be corrected for this change in shape.<sup>28</sup> The measured mobility diameters of dry NaCl particles ( $d_m$ ) were converted into diameters of volume-equivalent spheres ( $d_{ve}$ ) using eq 3, where  $\chi_{t,v}$  is the geometric shape factor (in the appropriate flow regime) and  $C_c(d)$  is the Cunningham slip correction factor.<sup>52</sup>

$$\frac{d_m}{C_c(d_m)} = \frac{d_{ve}\chi_{t,v}}{C_c(d_{ve})} \quad (3)$$

The shape-corrected growth factors were then calculated as follows (note the difference between eqs 1 and 4)

$$\text{GF}_{\text{corrected}} = \frac{d_{ve}^{\text{wet}}}{d_{ve}^{\text{dry}}} \quad (4)$$

For irregular particles,  $d_m$  is always larger than  $d_{ve}$  because they experience more drag compared to spherical particles of the same volume, and therefore  $\chi_{t,v} \geq 1$ . The Cunningham slip correction factor is a function of the Knudsen number ( $Kn$ ). This factor accounts for the fact that particles do not experience as much drag in the free molecular flow regime ( $Kn > 10$ ) as they do in the continuum flow regime ( $Kn < 0.1$ )

$$C_c(Kn) = 1 + Kn \left[ \alpha + \beta \exp\left(-\frac{\gamma}{Kn}\right) \right] \quad (5)$$

$$Kn = \frac{2\lambda}{d} \quad (6)$$

The empirical parameters  $\alpha$ ,  $\beta$ , and  $\gamma$  are 1.142, 0.558, and 0.999, respectively.<sup>53</sup> Parameter  $\lambda$  is the mean free path in air at 1 atm ( $\sim 65$  nm). For illustrative purposes, Table 1 lists calculated values of  $Kn$ ,  $d_{ve}$ , and  $\chi_{t,v}$  for several mobility-equivalent sizes of NaCl particles.

Figure 4 shows the shape-corrected growth curves for NaCl nanoparticles with mobility diameters of 9, 11, 14, and 17 nm. The dashed lines in Figure 4 indicate the predicted DRH values from the empirical power law determined by Biskos et al.<sup>29</sup> The

observed values of DRH are in good agreement with the previous measurements; the deviations are within the accuracy of the RH probes. We were also able to confirm the discrete nature of deliquescence of NaCl nanoparticles (reported in Figure 2 of ref 29), wherein a bimodal particle size distribution is observed in the immediate vicinity of the deliquescence transition.

Present measurements also confirm that postdeliquescence GF (that is, GF measured above the DRH point) decreases with decreasing dry diameter as a consequence of the Kelvin effect.<sup>30</sup> Table 2 shows the mobility GF (not corrected for the shape effects) for NaCl nanoparticles at 80% RH, when particles are already deliquesced. Within the experimental uncertainties, the GF values measured in this work for 9, 11, 14, and 17 nm particles, and in ref 28 for 6, 8, 10, 15, 20, 30, 40, and 60 nm particles increase monotonically with the particle mobility diameter. In summary, our tandem nano-DMA instrument correctly reproduces the shapes of the growth curves and the GF values for NaCl nanoparticles.

**Hygroscopic Growth of AOT/NaCl Nanoparticles.** Figure 5 shows the measured hygroscopic growth curves for 17 nm particles containing variable amounts of AOT and NaCl. Shape-corrected GFs for pure NaCl particles are included for reference. No shape correction is applied to the measured GF for mixed AOT/NaCl nanoparticles because they are assumed to be spherical. The particles are assumed to have the same relative weight fraction of AOT and NaCl as in the aqueous solution that is electrosprayed (the validity of this assumption will be discussed below). The 5 wt % AOT/NaCl (this notation means 5% AOT and 95% NaCl by weight) nanoparticles have a growth curve that is qualitatively similar to that of pure NaCl; however the DRH is reproducibly lower by approximately 3% RH and the postdeliquescence growth is suppressed. As the concentration of AOT increases, the apparent location of the deliquescence transition shifts to lower RH values and the GF values decrease in magnitude. The deliquescence of 5 and 25 wt % AOT/NaCl nanoparticles can be characterized as “prompt”; i.e., the transition happens over a relatively narrow range of RH. However, the 50 and 75 wt % AOT/NaCl nanoparticles deliquesce over  $\sim 5\%$  RH units. The 75 wt % AOT/NaCl nanoparticles show lower GF than 50 wt % AOT/NaCl nanoparticles at lower RH values (65–75% RH) and then converge to the same growth curve at higher values (75–86%). Pure AOT particles display negligible growth over this RH range.

Figure 6 shows measured hygroscopic growth curves for 9 nm AOT/NaCl particles (0 wt % AOT, 25 wt % AOT, and 100 wt % AOT). The growth curves of 9 and 17 nm 25 wt % AOT/NaCl particles are quite different. The most striking difference is the lack of discernible deliquescence transition in the 9 nm particles. A gradual uptake of water over the course of nearly 30% RH units is observed instead. The final growth factors are considerably suppressed in 9 nm particles as opposed to the 17 nm particles.

**Measurements for Bulk Mixtures.** To investigate bulk effects that added surfactants may have on hygroscopic interactions of NaCl and water, experiments were conducted in which RH was measured above saturated solutions of NaCl, NaNO<sub>3</sub>/NaCl, and AOT/NaCl. In all cases, a mixture of 20 g of solid and 10 mL of H<sub>2</sub>O was mixed in a 280 cm<sup>3</sup> sealed chamber. RH in the chamber was measured after it stabilized, typically some 24 h after the mixture was prepared. The results are summarized in Table 3. Mixing NaCl and NaNO<sub>3</sub> reduced the equilibrium RH, as expected.<sup>15</sup> On the contrary, the addition of

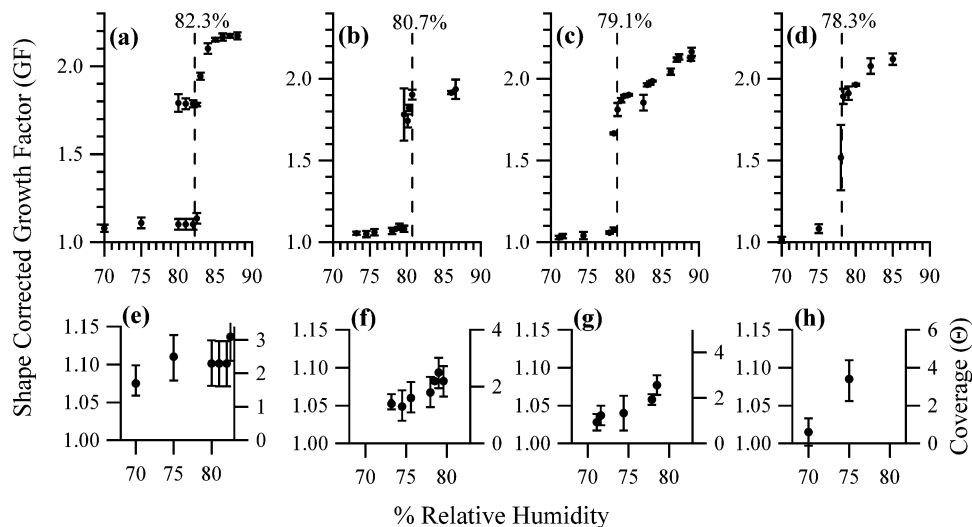


**Figure 4.** Shape-corrected growth curves ( $2\sigma$  errors) of pure NaCl nanoparticles:  $d_m =$  (a) 9 nm; (b) 11 nm; (c) 14 nm; (d) 17 nm. Special attention is given to the region before deliquescence for  $d_m = 9, 11, 14, 17$  nm particles in panels e, f, g, and h, respectively. Water monolayer coverage was calculated from the GF values as described in the text. The dashed lines are calculated DRH from ref 28.

**TABLE 2: Nanosize Effects on GF of NaCl Nanoparticles at 80% RH**

$d_m$ (nm)	mobility GF <sup>a</sup>	mobility GF <sup>b</sup>
6		1.45 <sup>c</sup>
8		1.55 <sup>c</sup>
9	1.57 ± 0.05	
10		1.55 <sup>c</sup>
11	1.52 ± 0.04	
14	1.66 ± 0.01	
15		1.68
17	1.71 ± 0.01	
20		1.71
30		1.74
40		1.76
60		1.75
∞		1.84

<sup>a</sup> This work;  $2\sigma$  error bars result from averaging repeated measurements. <sup>b</sup> From Biskos et al.<sup>28</sup> <sup>c</sup> Growth factor on the efflorescence branch in the vicinity of 80% RH.<sup>28</sup>

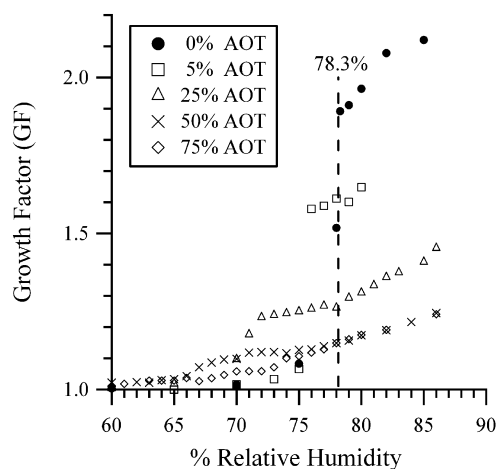


**Figure 5.** Measured growth curves for 17 nm AOT/NaCl particles for different wt % of AOT. The NaCl (0 wt % AOT) GF values are shape-corrected. The dashed line shows the expected DRH for 17 nm NaCl particles. Error bars are not shown to avoid congestion.

AOT to the saturated NaCl solutions had no effect on the equilibrium vapor pressure of water.

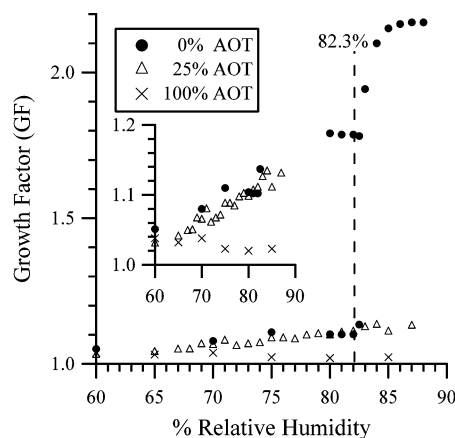


**Figure 6.** Measured growth curves for 9 nm AOT/NaCl particles for different wt % of AOT. Error bars are not shown to avoid congestion.

## Discussion

**Predeliquescence Wetting of NaCl Nanoparticles.** The theoretical interpretation for the nanosize effect on deliquescence of pure NaCl nanoparticles has been provided by Russell and Ming.<sup>22</sup> They considered a three-phase system consisting of water vapor, crystalline NaCl, and a thin layer of adsorbed surface water. They showed that for realistic values of the surface tension at the NaCl–air, NaCl–surface water, and surface water–air interfaces, a thin layer of adsorbed surface water increases the free energy of the wetted particle. This must be compensated by the corresponding increase in the free energy of the deliquesced particle

$$\Delta G^{\text{deliquescence}} = G_{\text{particle}}^{\text{deliquesced}} - G_{\text{particle}}^{\text{wetted}} = 0 \quad (7)$$

which in turn increases the water activity above the particle surface at the deliquescence point. This effect of the surface tensions on the deliquescence equilibrium becomes negligibly small for particles that are larger than 100 nm in size.

The existence of adsorbed H<sub>2</sub>O on the surface of NaCl below DRH is consistent with experimental observations in this and other laboratories. For example, previous measurements on bulk

TABLE 3: Water Activities above Saturated Solutions of AOT and NaCl<sup>a</sup>

mixture	description	measured % RH
NaCl	20 g of solid covered with 10 mL of H <sub>2</sub> O	76.0
NaNO <sub>3</sub> + NaCl (X <sub>NaCl</sub> = 0.40; eutonic mix)	20 g of solid covered with 10 mL of H <sub>2</sub> O	69.0
AOT + NaCl (X <sub>NaCl</sub> = 0.75)	20 g of solid emulsified with 10 mL of H <sub>2</sub> O	76.0
AOT + NaCl (X <sub>NaCl</sub> = 0.75)	20 g of solid covered with 10 mL of H <sub>2</sub> O	76.0
AOT + NaCl	20 g of solid NaCl covered with 10 mL of 0.5 g/L AOT solution	76.0

<sup>a</sup> X<sub>NaCl</sub> is weight fraction of NaCl.

NaCl showed that NaCl acquires 3–4 monolayers of water above 70% RH.<sup>46,48</sup> A tandem nano-DMA experiment conducted on 8–15 nm NaCl nanoparticles showed that the surfaces adsorb 0.5–2 monolayers of water between 40 and 60% RH.<sup>27</sup> Recent environmental TEM, ambient pressure XPS, and scanning force microscopy studies also revealed a layer of liquid-like water prior to deliquescence on NaCl surfaces.<sup>43–45,54</sup> The addition of 2 monolayers of water onto a 10 nm particle translates into a GF of approximately 1.05. This level of coverage with water is readily detectable in a tandem nano-DMA experiment (typical uncertainties in our GF measurements are on the order of  $\pm 2\sigma = \pm 0.02$ ). In contrast, the same level of coverage for a 1  $\mu$ m particle would correspond to GF of only 1.0005, which is not measurable with current mobility techniques.

Figure 4 shows the shape-corrected growth factors for  $d_m = 9, 11, 14,$  and 17 nm NaCl particles, with special attention paid to the region immediately before the deliquescence point. GF values were converted into effective coverage of water ( $\Theta_w$ ) by using eq 8.

$$\Theta_w = \frac{S_w}{S_{\text{NaCl}}} \quad (8)$$

$S_{\text{NaCl}} = 6.4 \times 10^{14} \text{ cm}^{-2}$  is the surface density of ion pairs for the NaCl(001) surface.<sup>55</sup> Surface concentration of adsorbed water,  $S_w$ , was calculated from  $d_{ve}$ , which were calculated from the experimentally determined values of  $d_m$  as described above.

$$S_w = \frac{N_w}{\pi(d_{ve}^{\text{dry}})^2} = \frac{\rho_w^{\text{mol}} \Delta V_{ve}}{\pi(d_{ve}^{\text{dry}})^2} = \frac{1}{6} \rho_w^{\text{mol}} d_{ve}^{\text{dry}} (\text{GF}^3 - 1) \quad (9)$$

In eq 9,  $N_w$  is the total number of adsorbed water molecules,  $\rho_w^{\text{mol}}$  is the molecular density of adsorbed water (33 molecules  $\text{nm}^{-3}$ ), and  $\Delta V_{ve}$  is the particle volume change due to the water adsorption.

The structure of water on a NaCl(001) surface was previously investigated by FTIR spectroscopy.<sup>46</sup> Researchers concluded that for  $\Theta_w \leq 0.5$ , water molecules aggregate into islands or clusters on the surface held together by hydrogen bonds and electrostatic surface attraction; at  $0.5 \leq \Theta_w \leq 2.5$  a transition region occurs with islands and a multilayer thin film; at  $2.5 \leq \Theta_w \leq 3.5$  a multilayer film with properties similar to those of bulk liquid water exists; and finally, the range  $\Theta_w \geq 3.5$  has been called the presolution region. Equating the water density to 33 molecules  $\text{nm}^{-3}$  (1.0 g  $\text{cm}^{-3}$ ) is therefore appropriate only at sufficiently large coverage. At low coverage levels, the  $\Theta_w$  values calculated from eqs 8 and 9 and shown in Figure 4 are likely to be overestimated. As water adopts on an icelike structure at low coverage levels, a more appropriate density in the low coverage regime should be somewhere between 30 and 33 molecules  $\text{nm}^{-3}$ . Despite the admittedly approximate treatment of the water uptake, the coverage levels predicted from

eqs 8 and 9 support the notion that the NaCl crystal is coated with several monolayers of water below the deliquescence transition.

**Hygroscopic Growth of 17 nm AOT/NaCl Particles.** Before discussing the hygroscopic growth of AOT/NaCl particles, we need to estimate the initial coverage of NaCl with AOT. This can only be done approximately because the details of structure, composition, and mobility of the AOT/NaCl particles generated by the electrospray source are not known. The first approximation that we have to make is that the relative amounts of NaCl and AOT in the nanoparticles are the same as those in the starting solution. The second assumption is that the AOT/NaCl nanoparticles have a spherical shape. This assumption is not likely to hold at very low AOT coverage levels, when there is not enough surfactant to significantly perturb the NaCl surface. Furthermore, AOT is likely to segregate into islands on NaCl at sub-monolayer coverage levels; this is similar to the behavior of fatty acids on surfaces.<sup>56,57</sup> However, with AOT coverage approaching a monolayer, it is reasonable to assume that the particles are uniformly coated with AOT and are close to spherical.

We also assume that AOT forms a film on the NaCl surface (as opposed to an internally mixed particle). This assumption is consistent with observations by Woods et al.<sup>58</sup> who examined morphology of the 70–100 nm NaCl particles containing ~5 wt % SDS (sodium dodecyl sulfate; another well-known surfactant) using a probe-molecule spectroscopy technique. In their experiments, the structure of the 70–100 nm 5 wt % SDS/NaCl particles above DRH was inverted-micelle-like; i.e., SDS was distributed on the surface with its nonpolar tails sticking out. Below the DRH, the morphology was consistent with a thin oily film of SDS on a solid salt crystal.

Our final assumption is that the AOT surface film is not porous; in other words, a rigid core–shell model is applicable to AOT/NaCl particles at a monolayer coverage level. Tsai et al.<sup>59</sup> showed that gold nanoparticles (10–60 nm) coated with self-assembled monolayers (SAMs) of alkanethiols appeared to have a “soft” organic coating. The SAM/Au particle size deduced from the mobility measurements was smaller than the size expected from purely geometric considerations.<sup>59</sup> We assume that the tapered shape of the AOT molecule will make the curved organic surface more compact, thus minimizing the effect of the organic coating on the physical diameter versus mobility diameter relationship.

With these approximations, the diameter of the NaCl core and the overall particle diameter can be related to each other in the following way

$$d_{\text{NaCl}} = \left( \frac{\text{wt}_{\text{NaCl}} \rho_{\text{AOT}} d_{\text{particle}}^3}{\rho_{\text{NaCl}} - (\rho_{\text{NaCl}} - \rho_{\text{AOT}}) \text{wt}_{\text{NaCl}}} \right)^{1/3} \quad (10)$$

$\text{wt}_{\text{NaCl}}$  is the weight fraction of NaCl in the solution,  $\rho_{\text{NaCl}}$  is the density of the NaCl core,  $\rho_{\text{AOT}}$  is the density of the AOT

**TABLE 4: Estimated Surface Coverage for 17 nm AOT/NaCl Particles**

wt % AOT <sub>sol</sub>	$d_{\text{NaCl}}$ (nm) <sup>a</sup>	anticipated $\Theta_{\text{AOT}}$ <sup>b</sup>	$\text{GF}_{\text{NaCl(core)}}(80\% \text{ RH})$ <sup>c</sup>	$\text{GF}_{\text{particle}}(80\% \text{ RH})$	apparent wt % AOT <sup>d</sup>	apparent $\Theta_{\text{AOT}}$ <sup>e</sup>
5.0	16.5	0.1	1.70	1.65	4.9	0.05
25	14.4	0.4	1.64	1.31	40	0.6
50	11.8	0.9	1.62	1.17	62	1.3
75	8.9	1.9	1.59	1.18	62	1.3

<sup>a</sup> Calculated from eq 10. <sup>b</sup> Calculated from eqs 11 and 12. <sup>c</sup> Estimated from data in Table 2. <sup>d</sup> Calculated from eq 14. <sup>e</sup> Calculated from apparent wt % AOT and eq 10 iteratively, third iteration is reported.

outer layer, and  $d$  stands for diameter. While it is reasonable to assume the bulk density for the NaCl core ( $2.165 \text{ g cm}^{-3}$ ), using the bulk density of AOT ( $1.1 \text{ g cm}^{-3}$ ) for the organic layer is likely to lead to an overestimation of the number of AOT molecules residing on the surface. Indeed, theoretical calculations predicted that a free AOT molecule can exist in seven conformations with an effective density ranging from 0.5 to  $1.0 \text{ g cm}^{-3}$ .<sup>60</sup> Neutron reflectivity measurements on AOT residing at the air–water interface showed that the lower limit for the area of an AOT head is  $0.78 \text{ nm}^2$ .<sup>61</sup> Treating AOT as a cylinder and using 1.3 nm as the chain length would then result in a density of  $0.74 \text{ g cm}^{-3}$ . As a compromise, we have adopted a value of  $\rho_{\text{AOT}} = 0.89 \text{ g cm}^{-3}$  for the effective density of the AOT outer shell.

Table 4 shows the results for the 17 nm AOT/NaCl particles with solution weight fractions of AOT ranging from 5 to 75 wt %. The AOT surface density and coverage were calculated as follows ( $N_{\text{AOT}}$  is the number of AOT molecules in the particle;  $N_a$  is the Avogadro number;  $\text{MW}_{\text{AOT}}$  is the molecular weight of AOT).

$$S_{\text{AOT}} = \frac{N_{\text{AOT}}}{\pi d_{\text{NaCl}}^2} = \frac{\rho_{\text{AOT}} N_a (d_{\text{particle}}^3 - d_{\text{NaCl}}^3)}{6 \text{MW}_{\text{AOT}} d_{\text{NaCl}}^2} \quad (11)$$

$$\Theta_{\text{AOT}} = \frac{S_{\text{AOT}}}{S_{\text{NaCl}}} \quad (12)$$

According to these calculations, the coverage exceeds a monolayer only after the weight fraction of AOT reaches a rather substantial level (>50 wt %). The 5 wt % and 25 wt % AOT/NaCl 17 nm particles have anticipated  $\Theta_{\text{AOT}}$  values of 0.1 and 0.4, respectively, leaving plenty of exposed NaCl sites for water vapor to interact with. The experimentally determined hygroscopic growth curves (Figure 5) are qualitatively consistent with the picture of a well-exposed NaCl surface sparingly covered with patches of AOT as a sharp deliquescence transition is observed followed by a substantial postdeliquescence growth to the particle.

In contrast, the 50 wt % and 75 wt % AOT/NaCl particles are predicted to have a much denser AOT overcoat, with an anticipated  $\Theta_{\text{AOT}} = 0.9$  and 1.9, respectively. These particles undergo deliquescence over a much broader range of RH values, likely as a result of heterogeneity in the structure of the AOT coating. AOT is likely to form aggregates at coverage levels exceeding one monolayer. The postdeliquescence growth is strongly suppressed reflecting the smaller amount of NaCl in these particles.

The reduction in both the GF and DRH values in AOT/NaCl is consistent with previous studies of hygroscopicity of surfactant-enriched NaCl particles.<sup>58,62,63</sup> The effect of the surfactant becomes more important as the particle size is reduced because of the larger surface energy contributions to the particle's free

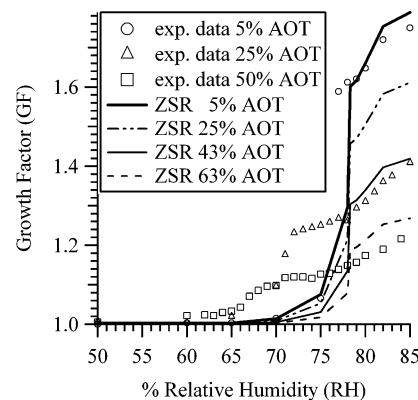


**Figure 7.** Predictions of the ZSR model compared to the experimental data for 17 nm AOT/NaCl particles.

energy. For example, the 70–100 nm NaCl/SDS particles studied by Woods et al.<sup>58</sup> contained more than enough SDS to completely coat the surface of NaCl. These particles deliquesced only 1% RH below the deliquescence point of pure NaCl particles. We observed no DRH suppression in bulk AOT/NaCl mixtures (Table 3). In contrast, the NaCl nanoparticles coated with a submonolayer of AOT experienced a very significant shift in the DRH (Figure 5).

In the ZSR (Zdanovskii–Stokes–Robinson) model, the hygroscopic GF of a multicomponent system is estimated from the known GF values of its pure components and their volume fractions.<sup>34,36,64,65</sup> The ZSR model assumes that there are no interactions among the different mixture components; therefore, the hygroscopic growth of the internally mixed particles is an appropriately weighed sum of the hygroscopic growth factors of its components.<sup>66</sup> It also assumes an ideal mixing behavior with spherical particles having a shape factor of unity.

Application of this model to AOT/NaCl particles predicts that GF should depend only on the volume fraction of NaCl ( $\epsilon_{\text{NaCl}}$ ) because pure AOT particles barely absorb any water and do not deliquesce in this RH range ( $\text{GF}_{\text{AOT}} \approx 1$ )

$$\text{GF}_{\text{particle}}^3 = \epsilon_{\text{NaCl}} \text{GF}_{\text{NaCl}}^3 + \epsilon_{\text{AOT}} \text{GF}_{\text{AOT}}^3 \approx 1 + \epsilon_{\text{NaCl}} (\text{GF}_{\text{NaCl}}^3 - 1) \quad (13)$$

It is clear that the ZSR model cannot account for the downward shift in the deliquesce transition of NaCl induced by the AOT coating (Figure 7). According to this model, the DRH should coincide with that of the NaCl core; i.e., it should occur at  $\geq 75\%$  RH. If the role of AOT were to merely reduce the available volume fraction of NaCl in the mixed AOT/NaCl particles, the DRH would actually go up as the fraction of AOT increased. The experimental observations display the opposite trend. This failure of the ZSR model is a direct consequence of strong interfacial interactions between NaCl and AOT; they clearly cannot be viewed as independent water adsorbers. The ZSR model also performs poorly in predicting the absolute magni-

**TABLE 5: Estimated Surface Coverage for 9 nm AOT/NaCl Particles**

wt % AOT <sub>sol</sub>	d <sub>NaCl</sub> (nm)	anticipated $\Theta_{\text{AOT}}$	GF <sub>NaCl(core)</sub> (80%RH)	GF <sub>particle</sub> (80% RH)	apparent wt % AOT	apparent $\Theta_{\text{AOT}}$
5.0	8.6	0.03	1.59			
25	7.4	0.2	1.58	1.10	74	1.0
50	6.0	0.5	1.56			
75	4.5	1.0	1.53			

tudes of the postdeliquescence GF values (Figure 7). While the model predictions for the 5 wt % AOT/NaCl particles are in fair agreement with the measured values, the model significantly overpredicts the measured GF values for the 25 wt % AOT/NaCl particles.

An alternative explanation for the overprediction of the postdeliquescence GF values by the ZSR model is that the relative volume fractions of AOT and NaCl in the particles are not the same as those in the original solution. In fact, the ZSR model can match the postdeliquescence data quite well if we assume that the particles are somehow enhanced with AOT relative to the solution used in the electrospray generator. For example, an application of the ZSR model to a 43 wt % AOT/NaCl mixture produces a reasonable agreement with the observed hygroscopic curves for the 25 wt % AOT/NaCl solution (Figure 7). This would imply an enhancement in AOT by nearly a factor of 2.

To further illustrate this point, Table 4 shows the surfactant enhancements in the 17 nm AOT/NaCl particles calculated under the assumption that the ZSR model is applicable at 80% RH. The GF<sub>NaCl(core)</sub> values for this calculation are estimated by fitting the combined NaCl hygroscopic growth data from Table 2 to an empirical power law. The apparent volume fraction of AOT is then computed from the measured GF<sub>particle</sub> values

$$\varepsilon_{\text{AOT}} = \frac{\text{GF}_{\text{NaCl(core)}}^3 - \text{GF}_{\text{particle}}^3}{\text{GF}_{\text{NaCl(core)}}^3 - 1} \quad (14)$$

and converted to apparent weight fraction of AOT as well as the apparent coverage layer. This calculation has to be done iteratively because the apparent coverage layer depends on the NaCl core diameter, which in turn depends on AOT weight fraction according to eq 10. This calculation is therefore repeated until convergence is achieved; the converged results are reported in Table 4. With the exception of the 5 wt % and 75 wt % AOT/NaCl cases, the nanoparticles appear to be enriched in AOT relative to the solutions from which they were generated. These results reflect complicated and still poorly understood dynamics of nanoparticle formation in electrospray sources.

**Hygroscopic Growth of 9 nm AOT/NaCl Particles.** Table 5 shows the predicted AOT surface coverage for 9 nm particles with AOT weight fractions ranging from 5 wt % to 75 wt %. These particles are only expected to attain monolayer coverage at 75 wt % AOT. The 25 wt % AOT/NaCl particles should have plenty of exposed NaCl sites for water adsorption, and a well-defined deliquescence transition can be expected by analogy with the 17 nm AOT/NaCl particles. Figure 6 demonstrates that this is not the case. Although the 25 wt % AOT/NaCl particles clearly increase in size more than pure AOT particles do, there is no clear deliquescence transition. The shape of the growth curve for 9 nm 25 wt % AOT/NaCl particles (anticipated  $\Theta_{\text{AOT}} = 0.2$ ) closely resembles that for 17 nm 75 wt % AOT/NaCl particles (anticipated to be fully coated with AOT). As in the 17 nm AOT/NaCl case, a possible explanation for this behavior is surfactant enhancement relative to the bulk solution that is

electrosprayed. Table 5 shows the results of the surfactant enhancement analysis similar to the one described above. In the 25 wt % AOT/NaCl 9 nm particles, calculations suggest surfactant enhancements that are 3-fold in the AOT wt % and 5-fold fold in the effective surface coverage.

Enhancement of surface active molecules in particles produced by electrospray sources is consistent with previous measurements. A study conducted by Tang and Smith<sup>67</sup> revealed that smaller satellite droplets and progeny droplets generated in electrospray are in fact surfactant-enriched. Although their experimental capabilities were qualitative and unable to directly quantify the level of enhancement, they estimate off-axis droplets could be as much as an order of magnitude larger in surfactant concentration compared to on-axis droplets from ion abundance in mass spectrometry analysis. The enrichment hypothesis definitively merits further theoretical and experimental investigation.

## Conclusions

We have constructed a tandem DMA apparatus and confirmed that it correctly captures the details of the hygroscopic growth of pure NaCl nanoparticles. The NaCl nanoparticles are observed to adsorb 1–4 monolayers of water below DRH. The deliquescence transitions in NaCl nanoparticles occur at well-defined DRH values, and the nanoparticles continue to take up water and grow above the DRH. The measured DRH values and growth factors are in quantitative agreement with previously published data. The DRH is shifted to lower values, and the growth factors are suppressed when the surfactant AOT is added to the nanoparticles. This effect is definitively particle size dependent; for example, no change in DRH of NaCl is observed for bulk AOT/NaCl mixtures. The ZSR model cannot explain the observed reduction in the DRH for the AOT/NaCl particles. This observation implies that there is in fact a cooperative interaction between NaCl, AOT, and water; the particle overall growth cannot be ascribed solely to the NaCl core. There is indirect evidence that the nanoparticles generated by the electrospray source are enriched in AOT compared to the electrosprayed aqueous solution.

**Acknowledgment.** This study was supported by the National Science Foundation through the Environmental Molecular Science Institute program, Grant CHE-0431312. Otto Dopfer is thankful to the Bavaria California Technology Center (BaCaTeC) for the travel exchange grant that supported his visit to UCI in 2007.

## References and Notes

- (1) Sioutas, C.; Delfino Ralph, J.; Singh, M. *Environ. Health Perspect.* **2005**, *113*, 947–955.
- (2) Geiser, M.; Rothen-Rutishauser, B.; Kapp, N.; Schurch, S.; Kreyling, W.; Schulz, H.; Semmler, M.; Im Hof, V.; Heyder, J.; Gehr, P. *Environ. Health Perspect.* **2005**, *113*, 1555–1560.
- (3) Oberdoerster, G.; Sharp, Z.; Atudorei, V.; Elder, A.; Gelein, R.; Kreyling, W.; Cox, C. *Inhalation Toxicol.* **2004**, *16*, 437–445.
- (4) Zhu, Y.; Hinds, W. C.; Kim, S.; Shen, S.; Sioutas, C. *Atmos. Environ.* **2002**, *36*, 4323–4335.

- (5) Kulmala, M.; Vehkamäki, H.; Petaja, T.; Dal Maso, M.; Lauri, A.; Kerminen, V. M.; Birmili, W.; McMurry, P. H. *J. Aerosol Sci.* **2004**, *35*, 143–176.
- (6) Pierce, J. R.; Adams, P. J. *Atm. Chem. Phys.* **2007**, *7*, 1367–1379.
- (7) Zhu, Y.; Hinds, W. C.; Shen, S.; Sioutas, C. *Aerosol Sci. Technol.* **2004**, *38*, 5–13.
- (8) Roeselova, M.; Jungwirth, P.; Tobias, D. J.; Gerber, R. B. *J. Phys. Chem. B* **2003**, *107*, 12690–12699.
- (9) Knipping, E. M.; Lakin, M. J.; Foster, K. L.; Jungwirth, P.; Tobias, D. J.; Gerber, R. B.; Dabdub, D.; Finlayson-Pitts, B. J. *Science* **2000**, *288*, 301–306.
- (10) Raymond, T. M.; Pandis, S. N. *J. Geophys. Res. D* **2002**, *107*, 4787 (doi: 4710.1029/2002JD002159).
- (11) Martin, S. T. *Chem. Rev.* **2000**, *100*, 3403–3453.
- (12) Cruz, C. N.; Pandis, S. N. *Environ. Sci. Technol.* **2000**, *34*, 4313–4319.
- (13) Cziczo, D. J.; Abbatt, J. P. D. *J. Phys. Chem. A* **2000**, *104*, 2038–2047.
- (14) Braban, C. F.; Carroll, M. F.; Styler, S. A.; Abbatt, J. P. D. *J. Phys. Chem. A* **2003**, *107*, 6594–6602.
- (15) Ge, Z.; Wexler, A. S.; Johnston, M. V. *J. Phys. Chem. A* **1998**, *102*, 173–180.
- (16) Liu, Y.; Yang, Z.; Desyaterik, Y.; Gassman, P. L.; Wang, H.; Laskin, A. *Anal. Chem.* **2008**, *80*, 633–642.
- (17) Tang, I. N.; Munkelwitz, H. R. *Atmos. Environ., Part A* **1993**, *27A*, 467–473.
- (18) Gao, Y.; Yu, L. E.; Chen, S. B. *J. Phys. Chem. A* **2007**, *111*, 633–639.
- (19) Hock, C.; Strassburg, S.; Haberland, H.; von Issendorff, B.; Aguado, A.; Schmidt, M. *Phys. Rev. Lett.* **2008**, *101*, 023401/023401–023401/023404.
- (20) Mirabel, P.; Reiss, H.; Bowles, R. K. *J. Chem. Phys.* **2000**, *113*, 8200–8205.
- (21) Djikavev, Y. S.; Bowles, R.; Reiss, H.; Haemeri, K.; Laaksonen, A.; Vaekevae, M. *J. Phys. Chem. B* **2001**, *105*, 7708–7722.
- (22) Russell, L. M.; Ming, Y. *J. Chem. Phys.* **2002**, *116*, 311–321.
- (23) Bahadur, R.; Russell, L. M. *Aerosol Sci. Technol.* **2008**, *42*, 369–376.
- (24) Bahadur, R.; Russell, L. M. *J. Chem. Phys.* **2008**, *129*, 094508/094501–094508/094510.
- (25) Hameri, K.; Laaksonen, A.; Vaekeva, M.; Suni, T. *J. Geophys. Res. D* **2001**, *106*, 20749–20757.
- (26) Hameri, K.; Vaekeva, M.; Hansson, H.-C.; Laaksonen, A. *J. Geophys. Res. D* **2000**, *105*, 22231–22242.
- (27) Romakkaniemi, S.; Haemeri, K.; Vaekevae, M.; Laaksonen, A. *J. Phys. Chem. A* **2001**, *105*, 8183–8188.
- (28) Biskos, G.; Russell, L. M.; Buseck, P. R.; Martin, S. T. *Geophys. Res. Lett.* **2006**, *33*, L07801 (doi: 07810.01029/02005GL025199).
- (29) Biskos, G.; Malinowski, A.; Russell, L.; Buseck, P.; Martin, S. *Aerosol Sci. Technol.* **2006**, *40*, 97–106.
- (30) Biskos, G.; Paulsen, D.; Russell, L. M.; Buseck, P. R.; Martin, S. T. *Atm. Chem. Phys.* **2007**, *6*, 4633–4642.
- (31) Bahadur, R.; Russell, L. M.; Alavi, S. *J. Phys. Chem. B* **2007**, *111*, 11989–11996.
- (32) Hansson, H. C.; Rood, M. J.; Koloutsou-Vakakis, S.; Hameri, K.; Orsini, D.; Wiedensohler, A. *J. Atmos. Chem.* **1998**, *31*, 321–346.
- (33) Choi, M. Y.; Chan, C. K. *Environ. Sci. Technol.* **2002**, *36*, 2422–2428.
- (34) Svenningsson, B.; Rissler, J.; Swietlicki, E.; Mircea, M.; Bilde, M.; Facchini, M. C.; Decesari, S.; Fuzzi, S.; Zhou, J.; Moenster, J.; Rosenoern, T. *Atmos. Chem. Phys.* **2006**, *6*, 1937–1952.
- (35) Salcedo, D. *J. Phys. Chem. A* **2006**, *110*, 12158–12165.
- (36) Wise, M. E.; Surratt, J. D.; Curtis, D. B.; Shilling, J. E.; Tolbert, M. A. *J. Geophys. Res. D* **2003**, *108*, 4638 (doi: 4610.1029/2003JD003775).
- (37) Abel, S.; Sterpone, F.; Bandyopadhyay, S.; Marchi, M. *J. Phys. Chem. B* **2004**, *108*, 19458–19466.
- (38) Kotlarchyk, M.; Chen, S. H.; Huang, J. S. *J. Phys. Chem.* **1982**, *86*, 3273–3276.
- (39) Zulauf, M.; Eicke, H. F. *J. Phys. Chem.* **1979**, *83*, 480–486.
- (40) Fuks, N. A. *Izv. Akad. Nauk SSSR, Ser. Geofiz.* **1964**, 579–586.
- (41) Wiedensohler, A. *J. Aerosol Sci.* **1988**, *19*, 387–389.
- (42) Fuks, N. A.; Sutugin, A. G. *Br. J. Appl. Phys.* **1963**, *14*, 39–42.
- (43) Wise, M. E.; Martin, S. T.; Russell, L. M.; Buseck, P. R. *Aerosol Sci. Technol.* **2008**, *42*, 281–294.
- (44) Wise, M. E.; Semeniuk, T. A.; Bruintjes, R.; Martin, S. T.; Russell, L. M.; Buseck, P. R. *J. Geophys. Res. D* **2007**, *112*, D10224 (doi: 10.1029/2006JD007678).
- (45) Wise, M.; Biskos, G.; Martin, S.; Russell, L.; Buseck, P. *Aerosol Sci. Technol.* **2005**, *39*, 849–856.
- (46) Foster, M. C.; Ewing, G. E. *J. Chem. Phys.* **2000**, *112*, 6817–6826.
- (47) Ewing, G. E. *Chem. Rev.* **2006**, *106*, 1511–1526.
- (48) Ewing, G. E. *J. Phys. Chem. B* **2004**, *108*, 15953–15961.
- (49) Verdaguier, A.; Sacha, G. M.; Luna, M.; Ogletree, D. F.; Salmeron, M. *J. Chem. Phys.* **2005**, *123*, 124703/124701–124703/124708.
- (50) Hemminger, J. C. *Int. Rev. Phys. Chem.* **1999**, *18*, 387–417.
- (51) Finlayson-Pitts, B. J. *Chem. Rev.* **2003**, *103*, 4801–4822.
- (52) DeCarlo, P.; Slowik, J.; Worsnop, D.; Davidovits, P.; Jimenez, J. *Aerosol Sci. Technol.* **2004**, *38*, 1185–1205.
- (53) Allen, M. D.; Raabe, O. G. *Aerosol Sci. Technol.* **1985**, *4*, 269–286.
- (54) Verdaguier, A.; Sacha, G. M.; Bluhm, H.; Salmeron, M. *Chem. Rev.* **2006**, *106*, 1478–1510.
- (55) *International Critical Tables of Numerical Data of Physics, Chemistry, and Technology*; Washburn, E. W., Ed.; published for National Research Council by McGraw-Hill Book Co.: New York, 1926.
- (56) Garland, E. R.; Rosen, E. P.; Clarke, L. I.; Baer, T. *Phys. Chem. Chem. Phys.* **2008**, *10*, 3156–3161.
- (57) Chakraborty, P.; Zachariah, M. R. *J. Phys. Chem. A* **2008**, *112*, 966–972.
- (58) Woods, E., III; Kim, H. S.; Wivagg, C. N.; Dotson, S. J.; Broekhuizen, K. E.; Frohardt, E. F. *J. Phys. Chem. A* **2007**, *111*, 11013–11020.
- (59) Tsai, D. H.; Zangmeister, R. A.; Pease, L. F., III; Tarlov, M. J.; Zachariah, M. R. *Langmuir* **2008**, *24*, 8483–8490.
- (60) Derecskei, B.; Derecskei-Kovacs, A.; Schelly, Z. A. *Langmuir* **1999**, *15*, 1981–1992.
- (61) Li, Z. X.; Lu, J. R.; Thomas, R. K. *Langmuir* **1997**, *13*, 3681–3685.
- (62) Chen, Y.-Y.; Lee, W.-M. G. *J. Environ. Sci. Health* **2001**, *A36*, 229–242.
- (63) Andrews, E.; Larson, S. M. *Environ. Sci. Technol.* **1993**, *27*, 857–865.
- (64) Dick, W. D.; Saxena, P.; McMurry, P. H. *J. Geophys. Res. D* **2000**, *105*, 1471–1479.
- (65) Varutbangkul, V.; Brechtel, F. J.; Bahreini, R.; Ng, N. L.; Keywood, M. D.; Kroll, J. H.; Flagan, R. C.; Seinfeld, J. H.; Lee, A.; Goldstein, A. H. *Atm. Chem. Phys.* **2006**, *6*, 2367–2388.
- (66) Stokes, R. H.; Robinson, R. A. *J. Phys. Chem.* **1966**, *70*, 2126–2131.
- (67) Tang, K.; Smith, R. D. *J. Am. Soc. Mass. Spectrom.* **2001**, *12*, 343–347.
- (68) Dahneke, B. E. *J. Aerosol Sci.* **1973**, *4*, 139–145.
- (69) Dahneke, B. E. *J. Aerosol Sci.* **1973**, *4*, 147–161.
- (70) Dahneke, B. E. *J. Aerosol Sci.* **1973**, *4*, 163–170.